Individual Variable Speed Limit Trajectory Control Considering Stochastic Arriving Patterns

Qianwen Li
University of South Florida
Handong Yao (handongyao@usf.edu)
University of South Florida https://orcid.org/0000-0002-2778-084X

S.I. : Integrated Development of Transportation and Energy

Keywords: Connected vehicles, speed advisory, signalized intersections, stochastic arriving pattern

Posted Date: February 8th, 2022

DOI: https://doi.org/10.21203/rs.3.rs-1288330/v1

Individual Variable Speed Limit Trajectory Control Considering Stochastic Arriving Patterns

Qianwen Li and Handong Yao*

Department of Civil and Environmental Engineering, University of South Florida, Tampa, Florida 33620

Abstract

Connected vehicles enabled by communication technologies have the potential to improve traffic mobility and enhance roadway safety such that traffic information can be shared among vehicles and infrastructure. Fruitful speed advisory strategies have been proposed to smooth connected vehicle trajectories for better system performance with the help of different car-following models. Yet, there has been no such comparison about the impacts of various car-following models on the advisory strategies. Further, most of the existing studies consider a deterministic vehicle arriving pattern. The resulting model is easy to approach yet not realistic in representing realistic traffic patterns. This study proposes an Individual Variable Speed Limit (IVSL) trajectory control problem at a signalized intersection and investigates the impacts of three popular car-following models on the IVSL. Both deterministic and stochastic IVSL models are formulated, and their performance is tested with numerical experiments. Results show that, compared to the benchmark (i.e., without speed control), the proposed IVSL strategy with a deterministic arriving pattern achieves significant improvements in both mobility and fuel efficiency across different traffic levels with all three car-following models. The improvement of the IVSL-Gipps' model is the most remarkable. When the vehicle arriving patterns are stochastic, the IVSL improves travel time, fuel consumption, and system cost by 8.95%, 19.11%, and 11.37%, respectively, as compared to the benchmark without speed control.

Keywords: Connected vehicles; speed advisory; signalized intersections; stochastic arriving pattern.

1. Introduction

Stop-and-go waves are frequently occurred at a signalized intersection due to a full stop, abrupt acceleration, and deceleration. And this can compromise traffic mobility, increase safety hazards, and cause a serious environmental effect. With the development of connected vehicle (CV) and connected autonomous vehicle (CAV), it is possible to obtain the traffic information (e.g., traffic signal timing, vehicle speed, acceleration), and communicate between vehicle and vehicle/infrastructure, then help/control vehicles to drive smoothly through advisory speed limit. Numerous speed control studies have been conducted to improve traffic efficiency, safety, and fuel economy, such as Optimal Speed Advisory (OSA) (Mahler and Vahidi 2012, Wan, Vahidi et al. 2016), Green Light Optimal Speed Advisory (GLOSA) (Katsaros, Kernchen et al. 2011, Nguyen, Kim et al. 2016), Eco-driving (Li, Wu et al. 2016, Jiang, Hu et al. 2017), Eco-Cooperative Adaptive Cruise Control (ECACC) (Kamalanathsharma and Rakha 2012, Rakha, Chen et al. 2016), Variable Speed Limit (VSL) (Ubiergo and Jin 2016) and trajectory smoothing (Ma, Li et al. 2017, Zhou, Li et al. 2017).

* Corresponding author。 E-mail: handongyao@usf.edu

CAV technologies (Nguyen, Kim et al. 2016, Rakha, Chen et al. 2016, Jiang, Hu et al. 2017, Ma, Li et al. 2017, Zhou, Li et al. 2017), however, can control detailed vehicles trajectories in high resolution, they are relatively future technologies and may not be implemented in near future. Therefore, this paper focuses on connected manned vehicles. In other words, vehicles in this study are controlled by human drivers, though with assistance from individual vehicle-based information provided by the connectivity technology. The majority of studies on speed control strategies have focused on the algorithms for generating optimized speed profiles or vehicular trajectories. However, in practice, the driver's behavior is stochastic, and it is difficult to predict the vehicle arriving patterns (i.e., arriving headway), and it is hard for a driver to exactly follow the optimal speed profiles or trajectories. To make these speed control strategies more realistic, some researches focused on driver's behavior based on eco-driving (Jamson, Hibberd et al. 2015, Pampel, Jamson et al. 2015, Xiang, Zhou et al. 2015, Li, You et al. 2016). Jamson and Hibberd proposed in-vehicle eco-driving assistance aiming to investigate the most effective and acceptable in-vehicle system for the provision of guidance on fuel-efficient accelerator usage (Jamson, Hibberd et al. 2015). Then, Hibberd studied the mental models of eco-driving that regular drivers have, and verified that in-vehicle guidance can increase driving safety compared to practicing eco-driving without them (Pampel, Jamson et al. 2015). Xiang developed a speed advisory model with driver's behavior adaptability for eco-driving, and it showed the proposed model can improve the fuel economy (Xiang, Zhou et al. 2015). Li proposed a modified stochastic model predict a control-based energy management strategy with considering driver's behavior to improve fuel economy (Li, You et al. 2016). Numerous researchers focused on the queue effect at a signalized intersection (He, Liu et al. 2015, Yang, Rakha et al. 2016). He presented a multi-stage optimal control formulation to obtain the fuel-optimal vehicle trajectory on signalized arterial accounting for both vehicle queue and traffic light status (He, Liu et al. 2015). Rakha developed an Eco-CACC algorithm considering queue effects to compute the fuel-optimum vehicle trajectory at a signalized intersection (Yang, Rakha et al. 2016). Others studied the stochastic problems at a signalized intersection (Sun and Liu 2015, Tong, Zhao et al. 2015). Tong utilized a stochastic programming model for oversaturated intersection signal timing, considering the uncertainty in traffic demand to minimize the vehicle delay (Tong, Zhao et al. 2015). Sun developed a stochastic eco-routing algorithm in a signalized traffic network, which incorporates the stochastic traffic light condition into the Markov decision process (MDP) (Sun and Liu 2015). Further, in our previous work, we proposed a trajectory smoothing method based on Individual Variable Speed Limits (IVSL) with location optimization at a signalized intersection (Yao, Cui, et al. 2018). Results show that the proposed IVSL strategy can greatly increase traffic efficiency and reduce fuel consumption.

In the above studies, car-following models were adopted to reproduce longitudinal human-driven vehicle behaviors, including Newell's model (Newell 2002), Gipps' model (Gipps 1981), and IDM model (Treiber, Hennecke et al. 2000). However, the impacts of different car-following models on IVSL have not been investigated. Also, limited efforts have been made to consider stochastic vehicle arriving patterns. Without considering realistic stochastic traffic patterns, the resulting speed control strategies might not be feasible in the real world. This study is motivated to address the two limitations. First, we compare three car-following models with the deterministic IVSL model. Then, we develop a two-stage stochastic IVSL optimization model considering the stochastic vehicle arriving patterns. The Monte-Carlo method (Metropolis and Ulam 1949) and the DIRECT algorithm (Jones 1993) are adopted to solve the stochastic IVSL model.

The rest of this paper is organized as follows. Section 2 introduces the Individual Variable Speed Limit (IVSL) trajectory control problem. Section 3 first presents three different car-following models in the IVSL control strategy. Next, a deterministic IVSL model is formulated, as

well as a two-stage stochastic IVSL model, which is integrated into the Monte-Carlo framework. Section 4 conducts numerical studies to test the model results. Section 5 concludes this paper and briefly discusses future research directions.

2. Problem Statement

This section introduces the IVSL trajectory control problem.

Road: As is shown in Figure 1, a single-lane segment leading to a signalized intersection has a length of L. The traffic signal is installed at the segment exit at location L, and the traffic moves from location 0 to location L.

Traffic Signal: A fixed signal timing with an effective green time length of G, an effective red time of R, and a signal cycle length of $C \coloneqq G + R$ are considered. Without loss of generality, the system is started from the beginning of a green phase at time 0.

Vehicles: Let $\mathbf{N} \coloneqq \{1,2,\cdots,N\}$ denote the set of all N vehicles. We assume that all vehicles have the same kinetic characteristics and do not move back. Let $x_n(t)$ denote the trajectory of vehicle n ($n \in \mathbf{N}$) at time t ($t \in [0,+\infty)$). Thus vehicle n's trajectory is x_n, and the set of all vehicle trajectories is denoted as $\mathbf{x} = \{x_n\}_{n \in N}$. The first-order differential $of\ \dot{x}_n(t)$ is the speed of vehicle n at time t. We require $\dot{x}_n(t) \in [0, v_{max}]$ where v_{max} is the maximum allowed speed on this segment. And the second-order differential of $\ddot{x}_n(t)$ is the acceleration of vehicle n at time t. With slight abuse of the math, define the inverse function $x_n^{-1}(l) \coloneqq argmin_t x_n(t) = l, \forall l \in [0, L]$. A subset of vehicles, denoted by $\mathbf{N}^C \subset \mathbf{N}$, are assumed to be equipped with an onboard unit that can receive real-time speed limits from the IVSLs while passing them.

Trajectory Control Measures: Two IVSLs, i.e., IVSL1 and IVSL2, are set along the segment at locations L_1 and L_2, respectively, where $0 \le L_1 \le L_2 \le L$. Each vehicle n proceeds in the following way before considering signals. Three car-following models are compared to show their impacts on IVSL strategies, such as Gipps' model, the modified Newell's model (M-Newell's model), and Intelligent Driver Model (IDM).

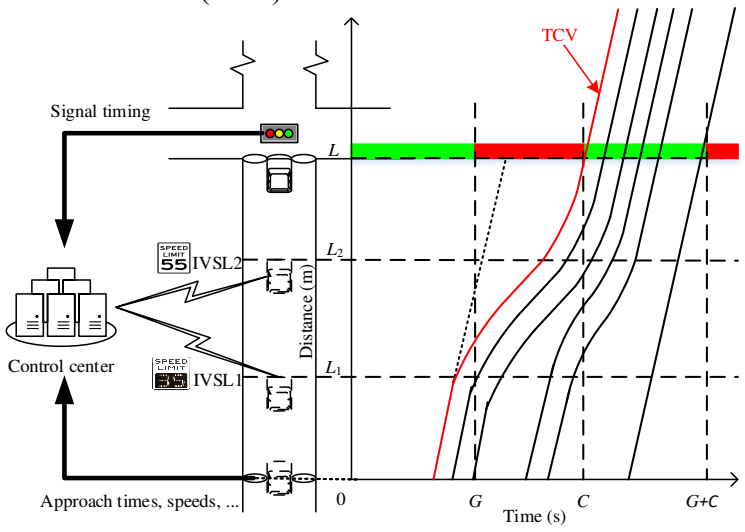

Figure 1 Illustration of the IVSL system.

This paper is an extension based on the previous work of Individual Variable Speed Limits with Location Optimization (Yao, Cui, et al. 2018). IVSL utilizes onboard devices with V2I communications to smooth vehicle trajectories and eliminate full stops at a signalized intersection. It allows dynamic adjustment of speed limits for an individual vehicle in response to real-time traffic states using in-vehicle displays. Figure 1 is the operations of the IVSL system. With the

IVSL system, a trajectory smoothing method is proposed to improve traffic efficiency and decrease vehicle fuel consumption and emissions. This method uses two individual IVSLs to guide vehicles on this highway segment (which would otherwise be held stopped at the current or following red light phase) to drive smoothly without a full stop (if possible) and just hit the beginning of the next green light. Note that IVSL essentially only needs to control some identified Target Control Vehicles (TCV) as lead vehicles of these platoons and the rest can be smoothed accordingly by just following the TCVs with their regular car-following behavior. In addition, noted that the queue effects of conventional vehicles and incompliant CV vehicles (i.e., compliance rate) are considered. Further, noted that the locations of these two IVSLs, i.e., IVSL1 and IVSL2, affect the smoothed trajectory shapes, and need to be carefully selected to optimize the overall traffic performance. Differ from the previous work, vehicle arriving patterns (i.e., arriving headway) are varied with different traffic conditions in a whole day, e.g., sparse traffic, intermediate traffic, and dense traffic. Thus, stochastic arriving patterns are considered into IVSLs optimization as a two-stage stochastic optimization problem, called Individual Variable Speed Limit with Stochastic Optimization (IVSL-SO). In reality, before installing the IVSL system, we can use historical data to estimate the vehicle trajectories with IVSL-SO and pre-set the IVSLs.

For convenience, Table 1 presents all indices and parameters used in this paper.

Table 1 Indices and Parameters.

$x_n(t)$	Location of the vehicle n. (m)
$\dot{x}_n(t)$	Speed of vehicle n. (m/s)
$\ddot{x}_n(t)$	Acceleration of vehicle n. (m/s^2)
$x_n^{-1}(l)$	Timestamp of vehicle n approaching location l.(sec)
s_n	Gap between vehicle n and $n-1$. (m)
s_n^*	Desired dynamical distance, especially in IDM. (m)
s_j	Minimum gap. (m)
L	Road segment length. (m)
L_1	Location of IVSL1. (m)
L_2	Location of IVSL2. (m)
h_n	Arriving headway between vehicle n and $n-1$. (m)
$\overline{v}_n$	Speed limit of vehicle n. (m/s)
$v_n^{L_1}$	Speed when each vehicle n hit the location L_1. (m/s)
v_n^+	Speed when each vehicle n pass the intersection. (m/s)
v_{max}	Maximum allowed speed. (m/s)
v_d	Desired speed. (m/s)
a	Maximum acceleration. (m/s^2)
d	Maximum deceleration. (m/s^2)
b	Comfortable deceleration, especially in IDM. (m/s^2)
a_n^{free}	Acceleration of free-flow traffic, especially in Gipps' model. (m/s^2)
a_n^{cong}	Acceleration of congested traffic, especially in Gipps' model. (m/s^2)
Δt	Time gap. (sec)
T	Safe time headway, especially in IDM. (sec)
τ	Sensitivity coefficient, especially in Gipps' model. (sec)
C	Signal cycle length. (sec)
G	Effective green time length. (sec)
R	Effective red time length. (sec)

t_{n1}	Time interval of deceleration from t_{n1}^{-} to t_{n1}^{+}. (sec)
t_{n2}	Time interval of vehicle n moving at speed limit $\overline{v}_n$ from t_{n2}^{-} to t_{n2}^{+}. (sec)
t_{n3}	Time interval of acceleration fromt_{n3}^{-} to t_{n3}^{+}. (sec)
t_n^{ms}	Starting timestamp of the merging process from free flow state to following state, especially in M-Newell's model. (sec)
t_n^{me}	Ending timestamp of the merging process from free flow state to following state, especially in M-Newell's model. (sec)
$TT(\mathbf{x})$	Measure 1, system travel time. (sec)
$FC(\mathbf{x})$	Measure 2, system fuel consumption. (liter)
δ	Acceleration exponent, especially in IDM.
K_{ij}	Coefficient matrix for VT-Micro model.
Ω	States set of traffic.
ST	State of sparse traffic.
IT	State of intermediate traffic.
DT	State of dense traffic.
k	Shape parameter of Weibull distribution function.
λ	Scale parameter of Weibull distribution function.
ω	Scenario.
N	Vehicle number.
M	Sample number.
p_{ST}	Probability of the sparse traffic in a whole day.
p_{IT}	Probability of the intermediate traffic in a whole day.
p_{DT}	Probability of the dense traffic in a whole day.

3. Methodology

This section first introduces three popular car-following models that can be used in IVSL. Next, IVSL models with a deterministic vehicle arriving pattern and a stochastic arriving pattern are formulated, respectively.

3.1. IVSL Car-following models

3.1.1. Gipps' model

A simplified Gipps' car-following model (Treiber and Kesting 2013) is formulated as follows:

$$\dot{x}_n(t+\Delta t) = F^{Gipp}\left(\dot{x}_n(t), \dot{x}_{n-1}(t), s_n(t)\right) \coloneqq min\left[\dot{x}_n(t) + a \times \Delta t, v_{max}, v_n^{safe}\left(s_n(t), \dot{x}_{n-1}(t)\right)\right]. \quad (1)$$

Where a is the maximum acceleration; Δt is the constant time gap; and $v_n^{safe}\left(s_n(t), \dot{x}_{n-1}(t)\right)$ defines the "safe speed" (the highest possible speed for vehicle n),

$$v_n^{safe}\left(s_n(t), \dot{x}_{n-1}(t)\right) = d \times \Delta t + \sqrt{d^2 \times \Delta t^2 + \dot{x}_{n-1}(t)^2 - 2d \times \left(s_n(t) - s_j\right)}. \quad (2)$$

Where d is the maximum deceleration, it's negative; $s_n(t) = x_{n-1}(t) - x_n(t)$ is the gap between vehicle n and $n-1$; and s_j is the minimum gap. To make the above car following law applicable to vehicle 1, we can simply set $\dot{x}_0(t) = v_{max}$, $s_1(t) = \infty, \forall t$. And we use a set of limitations defined by (Gipps 1981) to govern the acceleration of vehicles except for the TCV:

$$a_n^{free}(t) = 2.5 \times a \times \left(1 - \frac{\dot{x}_n(t)}{v_{max}}\right) \times \sqrt{0.025 + \frac{\dot{x}_n(t)}{v_{max}}}. \quad (3)$$

$$a_n^{cong}(t) = \frac{1}{\tau} \times \left[\frac{1}{\Delta t} \times \left(s_n(t) - s_j + \frac{\dot{x}_{n-1}(t)^2 - \dot{x}_n(t)^2}{2 \times d}\right) - \dot{x}_n(t)\right]. \quad (4)$$

$$\ddot{x}_n(t) = max\left\{d, min\left\{a_n^{free}(t), a_n^{cong}(t)\right\}\right\}. \quad (5)$$

Where $a_n^{free}(t)$ is the acceleration of free-flow traffic, $a_n^{cong}(t)$ is the acceleration of congested traffic, and τ is the sensitivity coefficient (1.2 sec).

Once the vehicle n arrives at location 0, if it is a compliant vehicle ($n \in \mathbf{N}^C$), we can identify whether it is a TCV through the following hypothesis test. The hypothesis is that vehicle n is not a lead vehicle, and thus its trajectory can be predicted according to the Gipps' car-following law up to the stop-line. If the exit time of vehicle n is in the middle of a green phase, i.e., $iC < x_n^{-1}(L) \leq G + iC, \exists i \in \{0,1, \dots\}$, then the hypothesis holds and vehicle n is not a TCV. In this case, vehicle n will proceed according to Gipps' car-following law without activating IVSL. Otherwise, vehicle n would hit a green light if it just follows the preceding vehicle, and it thus shall be labeled as a TCV whose trajectory needs to be smoothed by IVSL to pass the intersection at the beginning of the next green phase. If vehicle n is a TCV, in addition to being constrained by the car-following law, it receives a variable speed limit $\overline{v}_n$ at location L_1 and will decelerate to $\overline{v}_n$ from location L_1 if its speed is greater than $\overline{v}_n$. At location L_2, speed limit $\overline{v}_n$ is lifted, and vehicle n proceeds only according to Gipps' car-following law.

If vehicle n is a non-compliant vehicle, in addition to Gipps' car-following law, we check whether it needs to stop at a red light. First, we let vehicle n just follow Gipps' car-following law. If its exit time $x_n^{-1}(L)$ is in a red phase, then we have $x_n^{-1}(L) \in (i_n C + G, (i_n + 1)C]$ where $i_n \in \{0,1, \cdots\}$ denotes the cycle index for this red light violation. In this case, we set $\dot{x}_n(t) = \min\left\{F^{\text{Gipp}}\left(\dot{x}_n(t), \dot{x}_{n-1}(t), s_n(t)\right), F^{\text{Gipp}}\left(\dot{x}_n(t), 0, L - x_n(t)\right)\right\}$ when $t \leq (i_n + 1)C$ and $\dot{x}_n(t) = F^{\text{Gipp}}\left(\dot{x}_n(t), \dot{x}_{n-1}(t), s_n(t)\right)$ when $t > (i_n + 1)C$. Otherwise, if $x_n^{-1}(L)$ is green, then vehicle n only follows Gipps' car-following law. This case can be incorporated into the previous formulations by setting $i_n = -1$.

With all these operation rules, the system dynamics is described as follows:

$$\dot{x}_n(t + \Delta t) = \begin{cases} \min\left\{F^{Gipp}\left(\dot{x}_n(t), \dot{x}_{n-1}(t), s_n(t)\right), \max\{\overline{v}_n, \dot{x}_n(t) + d \times \Delta t\}\right\}, \text{if } x_n(t) \in [L_1, L_2]; \\ F^{Gipp}\left(\dot{x}_n(t), \dot{x}_{n-1}(t), s_n(t)\right), \text{otherwise}, \end{cases} \text{if } n \text{ is a TCV}. \quad (6)$$

$$\dot{x}_n(t + \Delta t) = \begin{cases} \min\left\{F^{Gipp}\left(\dot{x}_n(t), \dot{x}_{n-1}(t), s_n(t)\right), F^{Gipp}\left(\dot{x}_n(t), 0, L - x_n(t)\right)\right\}, \text{if } t \leq (i_n + 1)C; \\ F^{Gipp}\left(\dot{x}_n(t), \dot{x}_{n-1}(t), s_n(t)\right), \text{otherwise}, \end{cases} \text{if } n \text{ is not a TCV} \quad (7)$$

$$x_n(t + \Delta t) = x_n(t) + \dot{x}_n(t + \Delta t) \times \Delta t. \quad (8)$$

3.1.2. Modified Newell's model

A simplified Newell's car-following model is proposed by (Newell 2002) as follows:

$$x_n(t + \Delta t) = F^{Newell}\left(x_n(t), x_{n-1}(t)\right) \coloneqq \min\left\{x_{n-1}(t) - s_j, x_n(t) + v_{max} \times \Delta t\right\}. \quad (9)$$

Where s_j is the minimum safe distance, v_{max} is the maximum allowed speed and Δt is the time gap.

For a specific vehicle, if it can run in a state with the maximum allowed speed v_{max}, we say it is in a free-flow state, while if it has to run by following its tightly previous vehicle, it is defined to be in the following state. As shown in Figure 2, according to simplified Newell's car-following

model, if vehicle n runs in the following state when it enters the control area, we can derive its trajectory in cyan solid line by simply translating the trajectory of vehicle $n-1$. However, if vehicle n runs in the free-flow state when it enters, its trajectory can be depicted in the yellow solid line. After running in the free flow state for a while, vehicle n will switch into the following state. As illustrated in Figure 2, this state transition at the merging point between the yellow solid line and cyan solid line forms a "speed jump" rather than a smooth change, which is highlighted by a red circle. This phenomenon is not consistent with real-world situations.

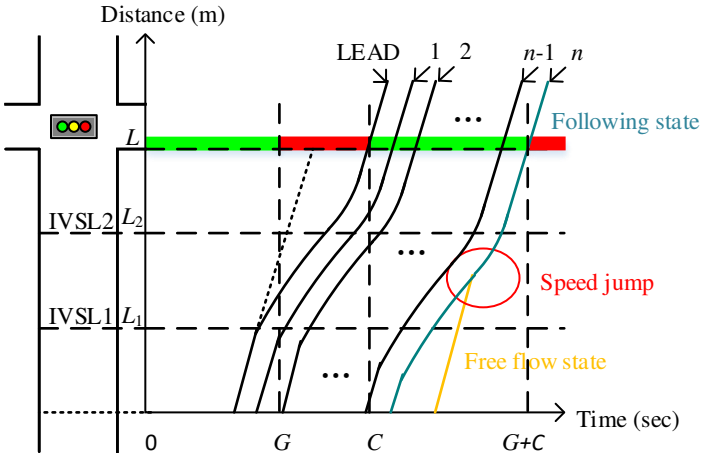

Figure 2 Time-space trajectory diagram of "speed jump".

Here, referring to the processing method of (Liu, Ghosal et al. 2012), we utilize two quadratic functions to smooth the state transition by approximating the original function at the merging point. The time-space trajectory diagram after processing is shown in Figure 3.

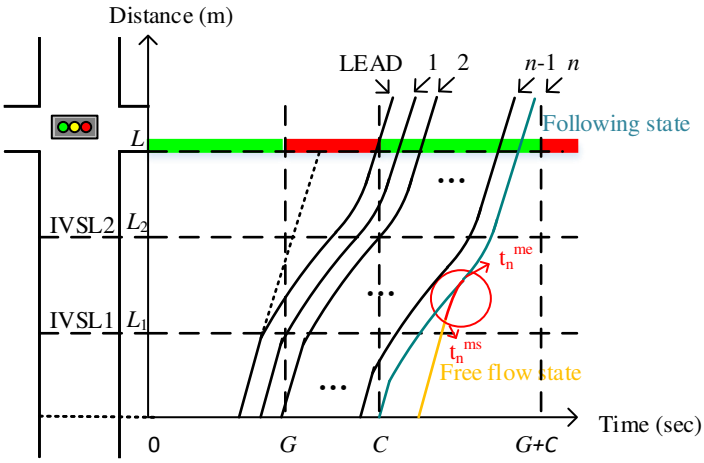

Figure 3 Time-space trajectory diagram after processing.

As is shown in Figure 3, for vehicle n, t_n^{ms} and t_n^{me} are the starting and ending timestamps of the merging process separately. Then, we can modify the simplified Newell's model, called M-Newell's model,

$$x_n(t+\Delta t) = F^{M-Newell}(x_n(t), x_{n-1}(t), t_n^{ms}, t_n^{me}) = \begin{cases} \dot{x}_n\left(x_n^{-1}(0)\right) \times \left(t - x_n^{-1}(0)\right) + 0.5 \times d \times \left(t - x_n^{-1}(0)\right)^2, & \text{if } t \in [t_n^{ms}, t_n^{me}], \\ \min\{x_{n-1}(t) - s_j, x_n(t) + v_{max} \times \Delta t\}, & \text{otherwise.} \end{cases} \quad (10)$$

So at the timestamp t_n^{me}, the speed and location of vehicle n should be equal to those derived by transferring the trajectory of vehicle $n-1$,

$$\begin{cases} \dot{x}_n(t_n^{ms}) + d \times (t_n^{me} - t_n^{ms}) = \dot{x}_n(t_n^{me} - \Delta t), \\ \dot{x}_n\left(x_n^{-1}(0)\right) \times \left(t_n^{me} - x_n^{-1}(0)\right) + 0.5 \times d \times (t_n^{me} - t_n^{ms})^2 = x_{n-1}(t_n^{me} - \Delta t) - s_j \end{cases}. \quad (11)$$

According to the simplified Newell's rule, the $n-1$ vehicle's trajectory can be translated from LEAD (the first vehicle in the platoon) vehicle's trajectory when the $n-1$ vehicle is at the following state, thus the Equation (11) can be rewritten as:

$$\begin{cases} \dot{x}_n(t_n^{ms}) + d \times (t_n^{me} - t_n^{ms}) = \dot{x}_{LEAD}(t_n^{me} - n \times \Delta t), \\ \dot{x}_n\left(x_n^{-1}(0)\right) \times \left(t_n^{me} - x_n^{-1}(0)\right) + 0.5 \times d \times (t_n^{me} - t_n^{ms})^2 = x_{LEAD}(t_n^{me} - n \times \Delta t) - n \times s_j \end{cases}. \quad (12)$$

To solve t_n^{ms} and t_n^{me} from Equation (12), three possible situations are considered:

1) If $t_n^{me} - n \times \Delta t \in t_{LEAD1}$, where t_{LEAD1} is the time interval of deceleration for LEAD vehicle. Equation (12) can be rewritten as:

$$\begin{cases} \dot{x}_n\left(x_n^{-1}(0)\right) + d \times (t_n^{me} - t_n^{ms}) = \dot{x}_{LEAD}\left(x_n^{-1}(0)\right) + d \times (t_n^{me} - n \times \Delta t - t_{LEAD1}^{-}), \\ \dot{x}_n\left(x_n^{-1}(0)\right) \times \left(t_n^{me} - x_n^{-1}(0)\right) + 0.5 \times d \times (t_n^{me} - t_n^{ms})^2 \\ = L_1 + \dot{x}_{LEAD}\left(x_n^{-1}(0)\right) \times (t_n^{me} - n \times \Delta t - t_{LEAD1}^{-}) + 0.5 \times d \times (t_n^{me} - n \times \Delta t - t_{LEAD1}^{-})^2 - n \times s_j. \end{cases} \quad (13)$$

Where t_{LEAD1}^{-} is the timestamp starting deceleration of LEAD vehicle.

2) If $t_n^{me} - n \times \Delta t \in t_{LEAD2}$, where t_{LEAD2} is the time interval of LEAD vehicle moving at the speed limit $\overline{v}_{LEAD}$ before hitting location L_2. Equation (12) can be rewritten as:

$$\begin{cases} \dot{x}_n\left(x_n^{-1}(0)\right) + d \times (t_n^{me} - t_n^{ms}) = \overline{v}_{LEAD}, \\ \dot{x}_n\left(x_n^{-1}(0)\right) \times \left(t_n^{me} - x_n^{-1}(0)\right) + 0.5 \times d \times (t_n^{me} - t_n^{ms})^2 \\ = L_1 + \dot{x}_{LEAD}\left(x_n^{-1}(0)\right) \times t_{LEAD1} + 0.5 \times d \times {t_{LEAD1}}^2 + \overline{v}_{LEAD} \times (t_n^{me} - n \times \Delta t - t_{LEAD2}^{-}) - n \times s_j. \end{cases} \quad (14)$$

Where t_{LEAD2}^{-} is the timestamp starting cruising during t_{LEAD2}.

3) If $t_n^{me} - n \times \Delta t \in t_{LEAD3}$, where t_{LEAD3} is the time interval of acceleration for LEAD vehicle. Equation (12) can be rewritten as:

$$\begin{cases} \dot{x}_n\left(x_n^{-1}(0)\right) + d \times (t_n^{me} - t_n^{ms}) = \overline{v}_{LEAD} + a \times (t_n^{me} - n \times \Delta t - t_{LEAD3}^{-}), \\ \dot{x}_n\left(x_n^{-1}(0)\right) \times \left(t_n^{me} - x_n^{-1}(0)\right) + 0.5 \times d \times (t_n^{me} - t_n^{ms})^2 \\ = L_1 + L_2 + \overline{v}_{LEAD} \times (t_n^{me} - n \times \Delta t - t_{LEAD3}^{-}) + 0.5 \times (t_n^{me} - n \times \Delta t - t_{LEAD3}^{-})^2 - n \times s_j. \end{cases} \quad (15)$$

Where t_{LEAD3}^{-} is the timestamp starting acceleration of LEAD vehicle.

In equations (13)-(15), only t_n^{ms} and t_n^{me} are variables, so by solving equations (13)-(15), we can get three combinations of t_n^{ms} and t_n^{me}. However, in practice, only one situation among the three can actually happen, so only one of the three solutions makes sense (i.e., only one solved t_n^{me} is consistent with its assumption condition). Once the starting timestamp t_n^{ms} and ending timestamp t_n^{me} of merging are got, we can derive the vehicle's trajectory with no "speed jump".

Thus, the system dynamics can be described with M-Newell's model as follows:

$$x_n(t + \Delta t) = \begin{cases} \min\left\{ \begin{matrix} F^{M-Newell}(x_n(t), x_{n-1}(t), t_n^{ms}, t_n^{me}), \\ \max\{x_n(t) + \overline{v}_n \times \Delta t, x_n(t) + \dot{x}_n(t) \times \Delta t + 0.5 \times d \times \Delta t^2\} \end{matrix} \right\}, \text{if } x_n(t) \in [L_1, L_2]; \\ F^{M-Newell}(x_n(t), x_{n-1}(t), t_n^{ms}, t_n^{me}), \text{ otherwise,} \\ \text{if } n \text{ is a TCV.} \end{cases} \quad (16)$$

$$x_n(t+\Delta t) = \begin{cases} \min\left\{ \begin{matrix} F^{M-Newell}(x_n(t), x_{n-1}(t), t_n^{ms}, t_n^{me}), \\ \max\{x_n(t) + \overline{v}_n \times \Delta t, x_n(t) + \dot{x}_n(t) \times \Delta t + 0.5 \times d \times \Delta t^2\} \end{matrix} \right\}, \text{if } t \le (i_n+1)C; \\ F^{M-Newell}(x_n(t), x_{n-1}(t), t_n^{ms}, t_n^{me}), \text{ otherwise,} \end{cases}$$

if n is not a TCV. (17)

$$\dot{x}_n(t+\Delta t) = \max\left(0, \left(x_n(t+\Delta t) - x_n(t)\right)/\Delta t\right). \quad (18)$$

$$\ddot{x}_n(t+\Delta t) = \left(\dot{x}_n(t+\Delta t) - \dot{x}_n(t)\right)/\Delta t. \quad (19)$$

3.1.3. IDM

IDM (Treiber, Hennecke et al. 2000) is presented in the following equations:

$$\ddot{x}_n(t) = F^{IDM}\left(\dot{x}_n(t), \dot{x}_{n-1}(t), s_n(t)\right) := max\left\{d, a \cdot \left[1 - \left(\frac{\dot{x}_n(t)}{v_d}\right)^{\delta} - \left(\frac{s_n^*(t)}{s_n(t)}\right)^2\right]\right\}, \quad (20)$$

$$s_n^*(t) = s_j + max\left\{0, \dot{x}_n(t) \cdot T + \frac{\dot{x}_n(t) \cdot [\dot{x}_n(t) - \dot{x}_{n-1}(t)]}{2 \cdot \sqrt{a \cdot |b|}}\right\}. \quad (21)$$

Where v_d is the desired speed, T is the safe time headway (1.6 sec), δ is the acceleration exponent (4, dimensionless), b is the comfortable deceleration.

The model is divided into a "desired" acceleration on a free road, and a braking acceleration induced by the preceding vehicle. The acceleration on a free road decreases from the initial maximum acceleration a to zero while the vehicle's speed approaches the specified speed limit, $\ddot{x}_n(t) = a \cdot \left[1 - (\dot{x}_n(t)/v_d)^{\delta}\right]$ is utilized to express the tendency of acceleration. The braking term is based on a comparison between the "desired dynamical distance" s_n^*, and the actual distance to the front vehicle. If the spacing is approximately equal to s_n^*, then the breaking acceleration part of the model essentially compensates for the free acceleration part, so the resulting acceleration is nearly zero.

And the system dynamics can be presented in the following equations:

$$\ddot{x}_n(t) = \begin{cases} \min\left\{F^{IDM}\left(\dot{x}_n(t), \dot{x}_{n-1}(t), s_n(t)\right), \max\{0, d\}\right\}, \text{if } x_n(t) \in [L_1, L_2]; \\ F^{IDM}\left(\dot{x}_n(t), \dot{x}_{n-1}(t), s_n(t)\right), \text{otherwise,} \end{cases}$$

if n is a TCV. (22)

$$\ddot{x}_n(t) = \begin{cases} \min\left\{F^{IDM}\left(\dot{x}_n(t), \dot{x}_{n-1}(t), s_n(t)\right), F^{IDM}\left(\dot{x}_n(t), 0, L - x_n(t)\right)\right\}, \text{if } t \le (i_n+1)C; \\ F^{IDM}\left(\dot{x}_n(t), \dot{x}_{n-1}(t), s_n(t)\right), \text{otherwise,} \end{cases}$$

if n is not a TCV. (23)

$$\dot{x}_n(t+\Delta t) = \max\left(0, x_n(t) + \ddot{x}_n(t) \times \Delta t\right). \quad (24)$$

$$x_n(t+\Delta t) = x_n(t) + \dot{x}_n(t+\Delta t) \times \Delta t. \quad (25)$$

3.2. Deterministic IVSL Optimization

Once the set of all trajectories $\mathbf{x} = \{x_n\}_{n \in N}$ is solved with car-following models, we use the following measures to evaluate the performance of the system. Essentially, all trajectories $\mathbf{x} = \{x_n\}_{n \in N}$ can be uniquely solved once locations L_1 and L_2 are given, and we thus denote these trajectories as functionals $\mathbf{x}(L_1, L_2)$. Therefore, all measures defined later depending on $\mathbf{x}$ can be equivalently denoted as functions of these two locations.

Measure 1: Travel Time (TT). For N vehicles, their total travel time which indicates the traffic efficiency is computed as follows:

$$TT(L_1, L_2) = \sum_{n=1}^{N}\left(x_n^{-1}(L) - x_n^{-1}(0)\right). \quad (26)$$

Measure 2: Fuel Consumption (FC). Based on the VT-micro vehicle fuel consumption and emission model (Ahn 1998), we can measure total fuel consumption as follows:

$$FC(L_1, L_2) = \sum_{n=1}^{N} \int_{x_n^{-1}(0)}^{x_n^{-1}(L)} exp\left\{\sum_{i=0}^{3}\sum_{j=0}^{3} K_{ij}\left(\dot{x}_n(t)\right)^i\left(\ddot{x}_n(t)\right)^j\right\} dt. \quad (27)$$

Where i and j are the power indexes, K_{ij} is a constant coefficient (Zegeye, De Schutter et al. 2013), $\dot{x}_n(t)$ means the first-order derivative of $x_n(t)$ (or velocity), and $\ddot{x}_n(t)$ means the second-order derivative of $x_n(t)$ (or acceleration). The coefficients matrix for $\{K_{ij}\}$ is shown in Table 2.

Table 2 Coefficients for fuel consumption (the unit of fuel consumption, speed, and acceleration are in $\mathbf{l/s}$, $\mathbf{m/s}$, and $\mathbf{m/s^2}$, respectively).

K_{ij}	$j=0$	$j=1$	$j=2$	$j=3$
$i=0$	-7.537	0.4438	0.1716	-0.0420
$i=1$	0.0973	0.0518	0.0029	-0.0071
$i=2$	-0.0030	-7.42E-4	1.09E-4	1.16E-4
$i=3$	5.3E-5	6E-6	-1E-5	-6E-6

For a given vehicle arriving pattern, locations of two IVSLs should be optimized with total travel time (TT) and total fuel consumption (FC) measures of this proposed IVSL method as stated above. The overall performance objective $SC(L_1, L_2)$ can be formulated as one of, a weighted summation of, or a vector of measures (26) and (27):

$$SC(L_1, L_2) = \varphi_T TT(L_1, L_2) + \varphi_F FC(L_1, L_2) \quad (28)$$

Weights φ_T and φ_F can be simply obtained as the dollar value of unit travel time and unit fuel consumption, respectively. Then, the IVSL location optimization problem can be formulated as follows:

$$\min_{L_1, L_2} SC(L_1, L_2) \quad (29)$$

s.t.

$$L - \frac{{v_{max}}^2}{2a} \le L_2 \le L. \quad (30)$$

$$0 \le L_1 \le L_2 - \frac{{v_{max}}^2}{2d}. \quad (31)$$

$$\text{and } \mathbf{x}(L_1, L_2) = \begin{cases} \{x_n\}_{n\in N, Gipps}, & \text{if subject to Equations (1) – (8);} \\ \{x_n\}_{n\in N, M-Newell}, & \text{if subject to Equations (9) – (19);} \\ \{x_n\}_{n\in N, IDM}, & \text{if subject to Equations (20) – (25).} \end{cases} \quad (32)$$

Constraint (30) confines the location of IVSL2 to this effective range. Although a feasible L_2 could be less than $L - {v_{max}}^2/2a$, the oscillation of vehicle trajectory is dependent on the deceleration/acceleration. The influence of acceleration is the same (i.e., $L_2 \le L - {v_{max}}^2/2a$ and $L_2 = L - {v_{max}}^2/2a$ yield the same optimal objective value) when $L_2 \le L - {v_{max}}^2/2a$, and the performance of the objective is independent of location L_2 whenever $L_2 \le L - {v_{max}}^2/2a$. Therefore, we just consider $L_2 \ge L - {v_{max}}^2/2a$ to simplify the formulation and improve optimization efficiency. Constraint (31) ensures there is enough spacing for a vehicle decelerating from v_{max} to any speed limit $\overline{v}_n$ imposed by IVSL1 before hitting IVSL2, and IVSL1 is set along the segment L. Constraint (32) means that the set of all the vehicles trajectories $\mathbf{x}(L_1, L_2) = \{x_n\}_{n\in N}$ are generated by the simulation described above with different car-following models (i.e., Equations (1) – (8) for Gipps' model, Equations (9) – (19) for M-Newell's model, and Equations (20) – (25) for IDM).

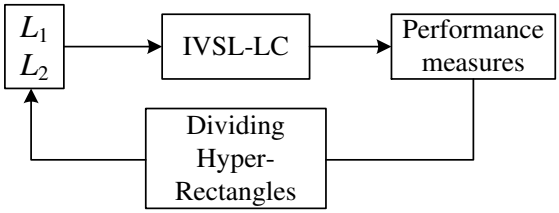

Figure 4 A typical iteration of the DIRECT algorithm.

Since this optimization problem is not necessarily monotone or convex, we have to numerically search for the optimal solution. To improve the search efficiency and the solution quality, instead of a linear search, we apply the DIRECT method for searching the global optimum. A typical iteration of the DIRECT algorithm integrating the IVSL based simulation is illustrated in Figure 4. For each candidate location of L_1 and L_2, the simulation is called to output the system performance measures. Then based on the evaluation of system performance, DIRECT decides the next candidate L_1 and L_2 values by dividing Hyper-Rectangles. This iteration will be repeated until the near-optimal solution of L_1 and L_2 is found. Please refer to Jones (1993) for the detail of this algorithm.

3.3. Two-Stage Stochastic IVSL Optimization

However, the vehicle arriving pattern (i.e., $\mathbf{h} = \{h_n\}_{n=2,3,\ldots,N}$, arriving headway set) is uncertain in practice, we need to develop a two-stage stochastic IVSL optimization (IVSL-SO) model considering the uncertain fluctuation in $\mathbf{h}$.

To better describe the uncertain vehicle arriving pattern, we assume $\mathbf{h}$ as a random variable vector whose probability distribution is known based on previous work. And it should be pointed out that an intersection experiences different demand levels at different times (e.g., a simple classification can include sparse traffic, intermediate traffic, and dense traffic) in a whole day. To be simplified, the set of three traffic demand levels in a whole day can be denoted as $\Omega = \{ST, IT, DT\}$ with a simple distribution: $Volume/Capacity = 0.32$ (sparse traffic) with probability p_{ST}, 0.68 (intermediate traffic) with probability p_{IT} and 0.84 (dense traffic) with probability p_{DT}, where $Volume$ is the traffic flow on a given road which can be described by $\mathbf{h}$, $Capacity$ is the maximum traffic flow on a given road, and p_{ST}, p_{IT}, p_{DT} is the probability of sparse traffic, intermediate traffic, and dense traffic, respectively. And we also set $p_{ST} + p_{IT} + p_{DT} = 1$.

According to (May 1990), it is assumed that $\mathbf{h}$ follows: 1) negative exponential distribution for sparse traffic; 2) Pearson Type III distribution for intermediate traffic; and 3) normal distribution for dense traffic. To compact the three different random distribution functions, Weibull distribution (Weibull 1951) with different parameters is employed here. The probability density function of the Weibull distribution is given below:

$$f^{weibull}(h;\lambda,k) = \begin{cases} \frac{k}{\lambda}\left(\frac{h}{\lambda}\right)^{k-1} e^{-(h/\lambda)^k}, & h \geq 0; \\ 0, & h < 0. \end{cases} \tag{33}$$

Where h is the continuous headway, and we can discrete it to $h_n = x_n(0) - x_{n-1}(0), n = 2,3,\ldots N$, i.e., the arriving headway between vehicle n and $n-1$, $k > 0$ is the shape parameter and $\lambda > 0$ is the scale parameter of the distribution. According to (Weibull 1951), the mean value is $\lambda\Gamma(1 + 1/k)$ where $\Gamma(\cdot)$ is the Gama function. Thus, when $k = 0.5$ and $\lambda = 2.125$, it is a negative exponential distribution (i.e., sparse traffic); when $k = 1.5$ and $\lambda = 1.0423$, it has a

similar shape with the Pearson Type III distribution (i.e., intermediate traffic); and when $k = 3$ and $\lambda = 0.4267$, it is the same shape as the normal distribution (i.e., dense traffic).

Since stochastic vehicle arriving headway is incorporated, we assume $\mathbf{h}$ as the random vector with known distribution subjected to Equation (33), and $\mathbf{h}^{\omega}$ as its realization under scenario ω.

Then, we extend the deterministic optimization model (29) into a two-stage stochastic optimization model. In the first stage master problem, we determine the location of L_1 and L_2, subject to the deterministic constraints on the allowable location setting range. In the second stage sub-problem, we evaluate the total travel time (TT) and the total fuel consumption (FC) measures of L_1 and L_2 under scenario ω.

The first stage of the stochastic optimization model considers the expected location of EL_1 and EL_2 is formulated as follows:

$$\min_{EL_1,EL_2} E[Q(L_1^{\omega}, L_2^{\omega}, \mathbf{h}^{\omega})]. \tag{34}$$

s.t.

$$L - \frac{{v_{max}}^2}{2a} \le EL_2 \le L. \tag{35}$$

$$0 \le EL_1 \le EL_2 - \frac{{v_{max}}^2}{2d}. \tag{36}$$

Where ω is a scenario which is included in Ω with three states, each state determines a distribution of $\mathbf{h}^{\omega}$; $Q(L_1^{\omega}, L_2^{\omega}, \mathbf{h}^{\omega})$ is the optimal objection function value of the second stage problem under first stage solution (EL_1,EL_2) and vehicle arriving headway set $\mathbf{h}$ under scenario ω; $E[Q(L_1^{\omega}, L_2^{\omega}, \mathbf{h}^{\omega})]$ is the expectation value.

According to Equation (33), the second stage scenario sub-problem can be formulated as follows:

$$Q(L_1^{\omega}, L_2^{\omega}, \mathbf{h}^{\omega}) = min_{L_1^{\omega}, L_2^{\omega}} SC(\mathbf{x}^{\omega}, \mathbf{h}^{\omega}). \tag{37}$$

s.t.

$$L - \frac{{v_{max}}^2}{2a} \le L_2^{\omega} \le L. \tag{38}$$

$$0 \le L_1^{\omega} \le L_2^{\omega} - \frac{{v_{max}}^2}{2d}. \tag{39}$$

$$\mathbf{x}^{\boldsymbol{\omega}}(L_1^{\omega}, L_2^{\omega}) = \{x_n^{\omega}\}_{n \in N, M-Newell}, \text{ subject to Equations (9) – (19).} \tag{40}$$

$$\mathbf{h}^{\omega} = \{h_n^{\omega}\}_{n=2,3,\dots,N} = \rho_{ST} \times f^{weibull}(h; 2.125, 0.5) + \rho_{IT} \times f^{weibull}(h; 1.0423, 1.5) + \rho_{DT} \times f^{weibull}(h; 0.4267, 3). \tag{41}$$

$$\rho_{ST} = \begin{cases} 1, & if\ \omega \in ST; \\ 0, & else. \end{cases} \tag{42}$$

$$\rho_{IT} = \begin{cases} 1, & if\ \omega \in IT; \\ 0, & else. \end{cases} \tag{43}$$

$$\rho_{DT} = \begin{cases} 1, & if\ \omega \in DT; \\ 0, & else. \end{cases} \tag{44}$$

$$ST = p_{ST} \times \Omega. \tag{45}$$

$$IT = p_{IT} \times \Omega. \tag{46}$$

$$DT = p_{DT} \times \Omega. \tag{47}$$

$$\Omega = \{ST, IT, DT\}. \tag{48}$$

$$p_{ST} + p_{IT} + p_{DT} = 1. \tag{49}$$

Where $(L_1^{\omega}, L_2^{\omega})$ is decision variables under scenario ω, and they must follow constraints (38) and (39). Constraint (40) depicts the set of all the vehicles trajectories $\mathbf{x}^{\boldsymbol{\omega}} \ge \{x_n^{\omega}\}_{n \in N, M-Newell}$ under scenario ω which are generated by the simulation with M-Newell's model described in Section 3 (i.e., Equations (9) – (19)). Constraints (41)-(49) describe the headway is generated by

the Weibull distribution function with different parameters according to three different traffic states, i.e., sparse traffic, intermediate traffic, and dense traffic.

One solution method of the two-stage stochastic optimization is to replace the expectation in the master problem with a sample mean estimator with a smaller size compared to the original sample space. And a common approach to reducing the scenario set to manageable sample size is using Monte Carlo simulation (Metropolis and Ulam 1949). In this paper, we generate a random sample and use the sample mean estimator to approximate the expectation in the original scenario space. Thus, the first stage master problem is approximated by the sample average,

$$\min_{\overline{L_1},\overline{L_2}} \frac{1}{M}\sum_{j=1}^{M} Q\left(L_1^j, L_2^j, \mathbf{h}^j\right). \tag{50}$$

s.t.

$$L - \frac{{v_{max}}^2}{2a} \le \overline{L_2} \le L. \tag{51}$$

$$0 \le \overline{L_1} \le \overline{L_2} - \frac{{v_{max}}^2}{2d}. \tag{52}$$

Where M is the number of samples, $\overline{L_1} = \frac{1}{M}\sum_{j=1}^{M} L_1^j$ and $\overline{L_2} = \frac{1}{M}\sum_{j=1}^{M} L_2^j$ are approximated to the expected locations EL_1 and EL_2, respectively.

This is also known as the Sample Average Approximation method. A typical framework of the Monte-Carlo method with the DIRECT algorithm integrating the IVSL is illustrated in Figure 5. And IVSL-SO is built on this framework to find the optimal sample average.

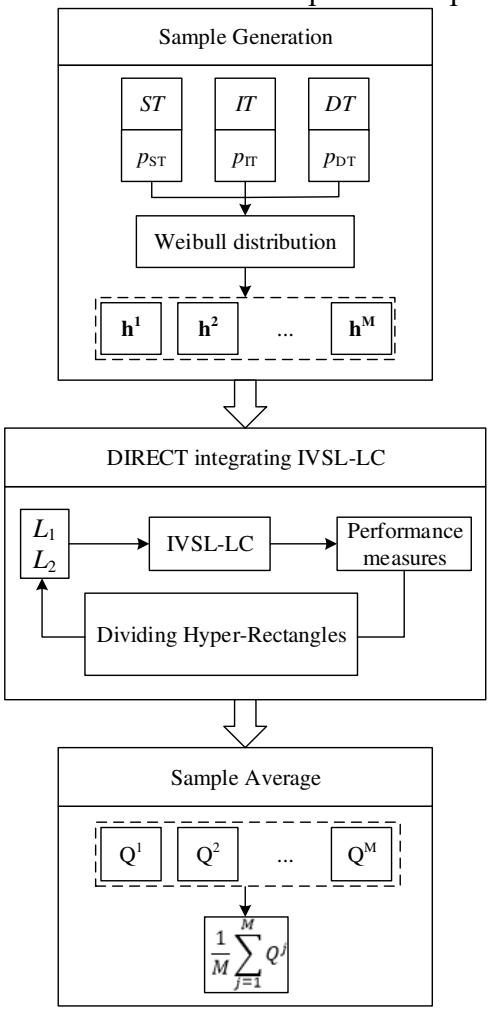

Figure 5 Framework of IVSL-SO system.

4. Numerical Experiments

In this section. We use numerical experiments to test the performance of the proposed IVSL models.

4.1. Deterministic optimization results

In this subsection. We use numerical experiments to test the performance of the deterministic IVSL with different car-following models. The parameters are set to the following values at default: $L = 800\text{m}$, $N = 60$, $s_j = 10\text{m}$, $\Delta t = 1$ sec, $v_{max} = 16\,\text{m/s}$, $\dot{x}_1\left(x_1^{-1}(0)\right) = v_{max}$, $a = 2\,\text{m/s}^2$, $d = -3\,\text{m/s}^2$, $G = 50$ sec, $C = 100$ sec, $\varphi_T = 20\,\$/\text{hour}$, $\varphi_F = 1\,\$/\text{liter}$, $\tau = 1.2\text{sec}$, $v_d = 16m/s$, $T = 0.85s$, $b = -3\,\text{m/s}^2$, $\delta = 4$ and the saturation time headway is 2sec.

Table 3 and Figure 6 show the comparison results for IVSL with three different car-following models depending on the traffic levels. And the measurements include the system travel time (min), the system fuel consumption (liter), the system cost ($), and solution time (sec). In Table 3, IVSL-Gipps', IVSL-M-Newell, and IVSL-IDM represent IVSL with Gipps' model, the modified Newell's model, and IDM, respectively. All three models are used in the joint optimization to optimize the system cost which is combined by travel time and fuel consumption. Table 3 shows the results under control and without control (i.e., benchmark, which is shown in parenthesis). And Figure 6 presents the increment rate of IVSL with three car-following models compared to the benchmark, respectively.

Table 3 Results comparison for three different car-following models.

		IVSL-Gipps'/benchmark	IVSL-M-Newell	IVSL-IDM
Sparse traffic	Travel time (min)	72.52 /75.55	72.37 (74.93)	79.33 (84.30)
	Fuel consumption (liter)	7.06 (8.30)	7.56 (7.97)	7.52 (8.29)
	System cost ($)	31.23 (33.49)	31.69 (32.94)	33.96 (36.39)
	Solution time (sec)	357.00	94.12	220.69
Intermediate traffic	Travel time (min)	84.48 (93.20)	84.28 (91.82)	104.30 (110.67)
	Fuel consumption (liter)	8.04 (10.33)	8.07 (9.72)	8.04 (10.09)
	System cost ($)	36.18 (41.40)	36.17 (40.33)	42.81 (46.98)
	Solution time (sec)	319.63	100.64	255.16
Dense traffic	Travel time (min)	106.02 (114.47)	105.85 (113.08)	126.17 (131.93)
	Fuel consumption (liter)	9.12 (12.30)	9.02 (11.49)	9.06 (11.43)
	System cost ($)	44.46 (50.46)	44.30 (49.18)	51.10 (55.41)
	Solution time (sec)	346.88	99.99	214.68

As is shown in Table 3 and Figure 6, with all three car-following models, the IVSL strategy can achieve significant improvements in both mobility and environments as the traffic level increases. The effect of the IVSL-Gipps' model is the most remarkable. This is probably because that Gipps' model has more parameters than IDM and M-Newell's model to reflect the vehicular dynamic, thus it can be more accurate to present the effect of IVSL strategy. And the tendency of the IVSL-Gipps' model and IVSL-M-Newell's model are approximately the same, but IVSL-IDM is totally different in Figure 6 (a) and (b), moreover the results of IVSL-IDM is a little higher than IVSL-Gipps' and IVSL-M-Newell in Table 3. This is probably due to the instability of IDM, i.e., the oscillation of speed occurs in the free-flow state. Then we assume traffic level in a whole day follows a specific distribution (i.e., the probability of intermediate traffic, sparse traffic, and dense traffic are 1/2, 1/4, and 1/4, respectively). And we can calculate the average increment rate of the system cost per day, which is 10.96% for the IVSL-Gipps' model, 8.59% for the IVSL-M-Newell's model, and 8.05% for the IVSL-IDM. That means IVSL-Gipps' model has the best performance, and IVSL-M-Newell's model is a little worse than IVSL-Gipps' model. On the other hand, IVSL-Gipps' model and IVSL-IDM cost more solution time than IVSL-M-Newell's model (about 2-4 times). As explained above, models with more parameters may cost higher solution time.

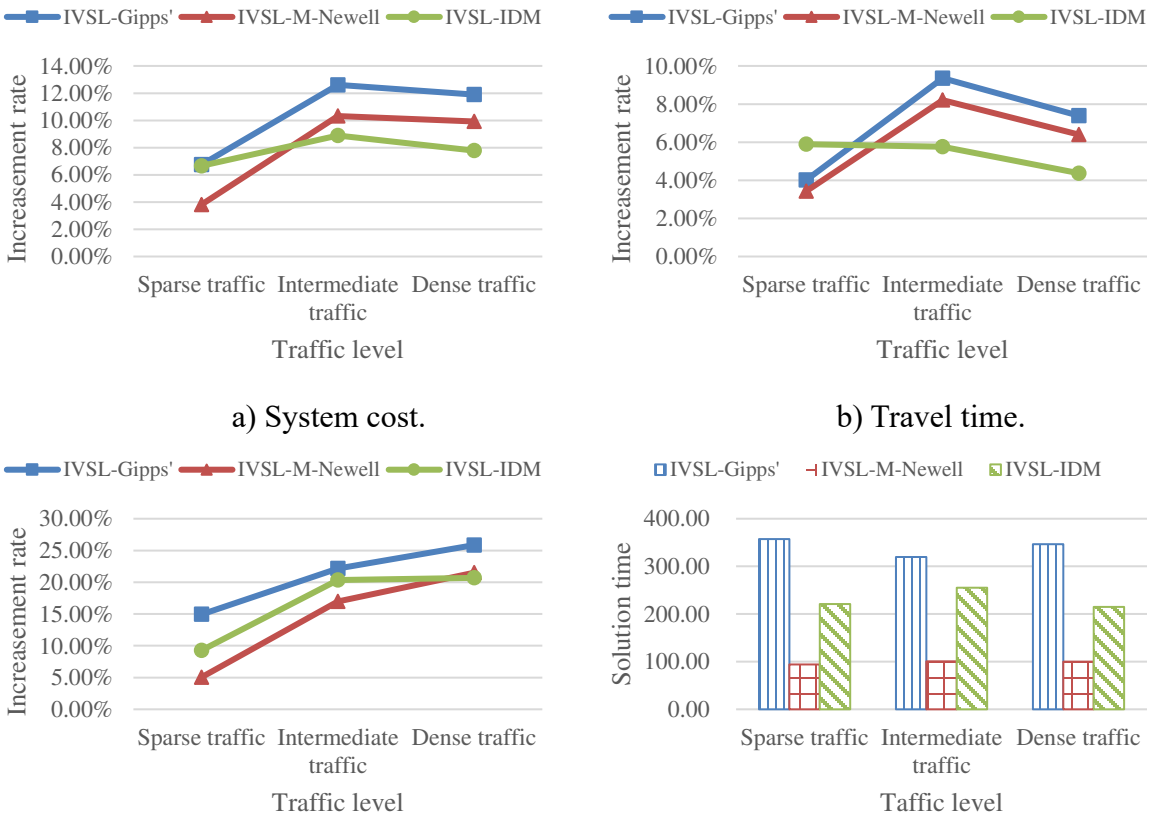

Figure 6 Comparison results of IVSL with three different car-following models.

4.2. Stochastic optimization results

This subsection conducts numerical experiments to test the performance of the stochastic IVSL (i.e., IVSL-SO). The parameters are set to the following values at default: $L = 800$m, $N = 60$,

$s_j = 10\text{m}$, $\Delta t = 1\,\text{sec}$, $v_{max} = 16\,\text{m/s}$, $\dot{x}_1\left(x_1^{-1}(0)\right) = v_{max}$, $a = 2\,\text{m/s}^2$, $d = -3\,\text{m/s}^2$, $G = 50\,\text{sec}$, $C = 100\,\text{sec}$, $\varphi_T = 20\,\$/\text{hour}$, $\varphi_F = 1\,\$/\text{liter}$, $p_{ST} = 0.25$, $p_{IT} = 0.5$, $p_{DT} = 0.25$. In Section 4.2.1, we vary the sample number M from 100 to 5000 to test the performance of the Monte-Carlo method. And in Section 4.2.2, according to the analysis in Section 4.2.1, we set a suitable sample number to investigate the performance of IVSL-SO.

4.2.1. Monte-Carlo sample test

This section investigates the performance of the Monte-Carlo method with the DIRECT algorithm integrating the IVSL for selecting a suitable sample range. Here, we firstly use the Monte-Carlo method to generate 5000 samples, and then the Pauta criterion (Xiao 1980) is presented to remove the worse samples (the final sample number is 4955). The performance results of 4955 samples are shown in Figure 7.

. It illustrates that IVSL1 is located in the range between 0 and 100m, IVSL2 is set in the range between 730 and 790m, and the optimal value oscillates from 26 to 45$ after the proposed optimization. And the color probability distribution follows the probability distribution of the traffic demand level in a whole day, i.e., the hotter one denotes the dense traffic, the colder one represents the sparse traffic, and the more part shows the probability of the intermediate traffic. These results demonstrate that the sample average can present a credible value due to a short fluctuation range. Thus, we can select the IVSLs according to this value.

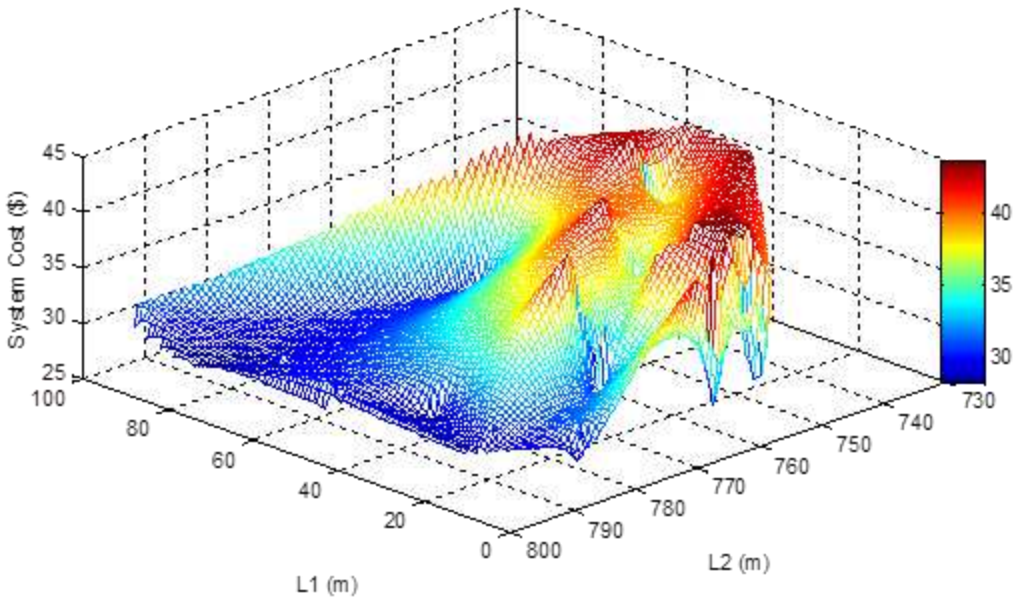

Figure 7 The performance results of 4955 samples.

Next, Table 4 and Figure 8 present the performance of the Monte-Carlo method with varied sample numbers (i.e., 100, 500, 1000, 4955). $\overline{TT}$ is the sample average of the system travel time, $\overline{FC}$ is the sample average of the system fuel consumption, $\overline{SC}$ is the sample average of the system cost, $\overline{L_1}$ is the sample average of the IVSL1's location, and $\overline{L_2}$ is the sample average of the IVSL2's location. And SD_$\overline{TT}$, SD_$\overline{FC}$, SD_$\overline{SC}$, SD_$\overline{L_1}$, and SD_$\overline{L_2}$ denote the standard deviation of $\overline{TT}$, $\overline{FC}$, $\overline{SC}$, $\overline{L_1}$, and $\overline{L_2}$, respectively. In the Monte-Carlo method, the sample average is utilized to approximate the expected value.

Table 4 Performance of Monte-Carlo method with various sample numbers.

Sample number	100	500	1,000	4955
$\overline{TT}$ (min)	87.16	86.54	86.58	86.70
SD_$\overline{TT}$	2.49	1.42	1.05	0.49
$\overline{FC}$ (liter)	7.84	7.85	7.86	7.86
SD_$\overline{FC}$	0.07	0.04	0.03	0.01
$\overline{SC}$ ($)	36.89	36.70	36.72	36.76
SD_$\overline{SC}$	0.90	0.50	0.37	0.17
$\overline{L_1}$ (m)	14.27	12.60	12.95	12.24
SD_$\overline{L_1}$	4.84	2.27	1.65	0.79
$\overline{L_2}$ (m)	764.26	763.15	762.50	762.82
SD_$\overline{L_2}$	1.89	0.96	0.81	0.46

As is shown in Table 4 and Figure 8, the expected measurements (including travel time, fuel consumption, and joint system cost), as well as the expected locations (including IVSL1 and IVSL2), become stable as the sample number increases. And $\overline{TT}$ is more susceptible than $\overline{FC}$ and $\overline{SC}$ to the varied sample number. In Figure 8 b), $\overline{L_1}$ is almost stable below 500 samples, and $\overline{L_2}$ is obviously fluctuant when the sample number is under 500. This is probably because that $\overline{L_1}$ is set to apply a speed limit value to the vehicle for deceleration, $\overline{L_2}$ is set to remove the speed limit value for acceleration, and the acceleration operation has a more obvious effect on system measurements (especially, travel time), and this makes sense why $\overline{TT}$ is more susceptible. From the above analyses, the sample number is set as 500 in the following part.

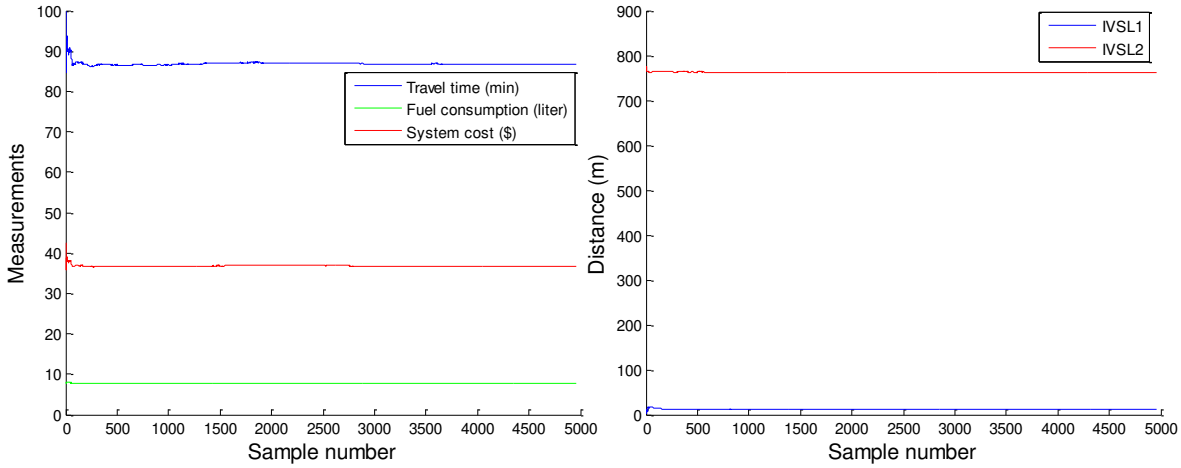

a) Expected measurements ($\overline{TT}$, $\overline{FC}$, $\overline{M}$). b) Expected locations ($\overline{L_1}$, $\overline{L_2}$).

Figure 8 Performance of Monte-Carlo method with various sample numbers.

4.2.2. Performance of IVSL-SO

In this section, we set the sample number equal to 500 to investigate the performance of IVSL-SO. According to subsection 4.2.1, we can obtain the sample average through the Monte-Carlo method. Then, we can apply random sampling (M=500) from the total sample set (the total sample number is 4955), which follows the distribution of $\Omega = \{ST, IT, DT\}$. After a random sampling, a sample average is obtained. Subsequently, we set the sampling frequency as 500,000 to get the optimal sample average through the Monte-Carlo method.

The stochastic optimization of IVSL's location requires a fast computation speed. As a result, IVSL-M-Newell's model is chosen to be embedded in the Monte-Carlo simulation because it is the most computationally efficient as compared to IVSL-Gipps' model and IVSL-IDM.

Figure 9 shows the convergence result of IVSL-SO. We can find that the convergence result is excellent. And after 500,000 sampling frequencies, the optimal expected system cost converges to stable as $\overline{SC}^*$ =36.00$, and the optimal expected locations are $\overline{L_1}^*$ =12.73m and $\overline{L_2}^*$ =762.51m.

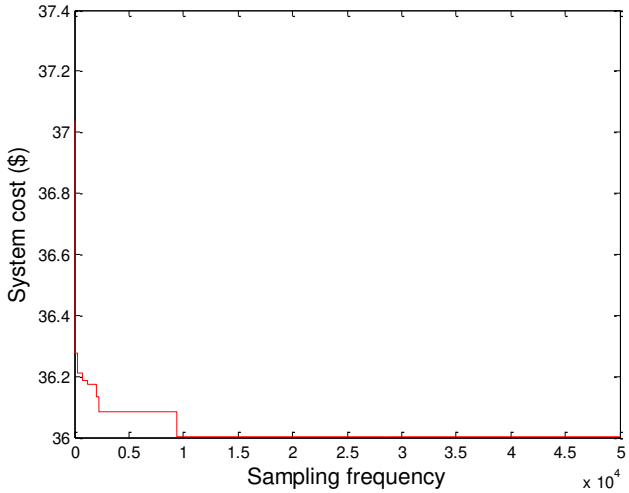

Figure 9 Convergence result of IVSL-SO.

Table 5 shows the comparison results between IVSL-SO and Benchmark (i.e., without control). After 10,000 sampling frequencies, the performance of the Benchmark is $\overline{SC}^B$ =40.62$, $\overline{FC}^B$=9.67liter and $\overline{TT}^B$=80.15min. Thus, the improvement of travel time, fuel consumption, and system cost is 8.95%, 19.11%, and 11.37%, respectively.

Table 5 Comparison result between IVSL-SO and Benchmark.

	Benchmark	IVSL-SO	Improvement
$\overline{TT}$ (min)	92.86	84.55	8.95%
$\overline{FC}$ (liter)	9.67	7.82	19.11%
$\overline{SC}$ ($)	40.62	36.00	11.37%

Figure 10 shows the time-space trajectories with/without control under specific scenarios, i.e., sparse traffic, intermediate traffic, and dense traffic. Overall, we can see, IVSL-SO can exactly eliminate full stops as we expected no matter which demand level is loaded. When no extra control is imposed on the vehicle platoon except for the regular signal control (i.e. Benchmark), vehicles inevitably suffer from full stops. Figure 10 a), b) and c) show that increasing the demand level will incur more full stops, which is intuitive since longer waiting in front of the red signal results from a higher demand level. Especially, in Figure 10 c), stop times increase to 2 or 3. Whereas, we see that IVSL-SO can well balance trajectory smoothing and queuing adjustment such that all vehicles can drive smoothly to the extent of not having full stops. This evidences the efficient performance of the IVSL-SO system.

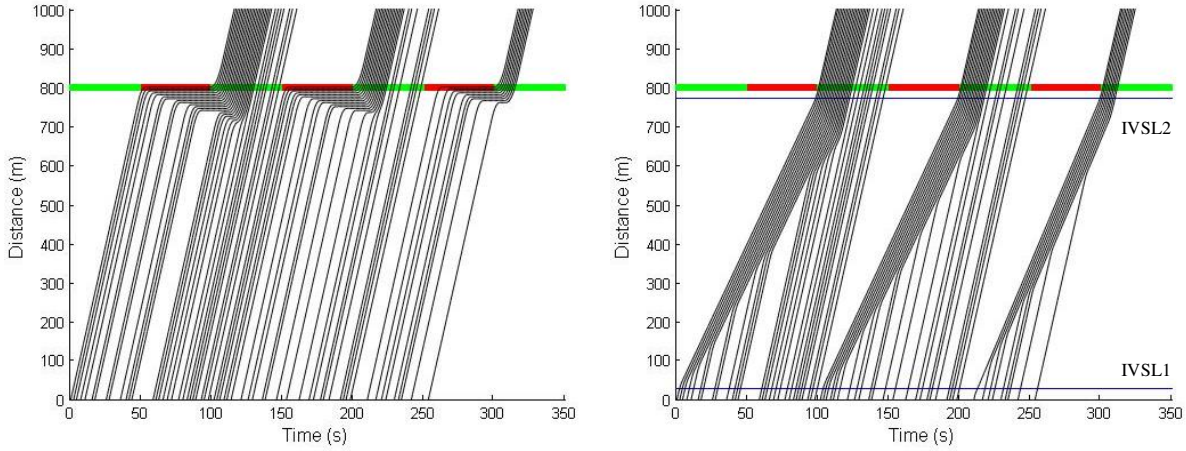

Benchmark IVSL-SO

a) Sparse traffic scenario.

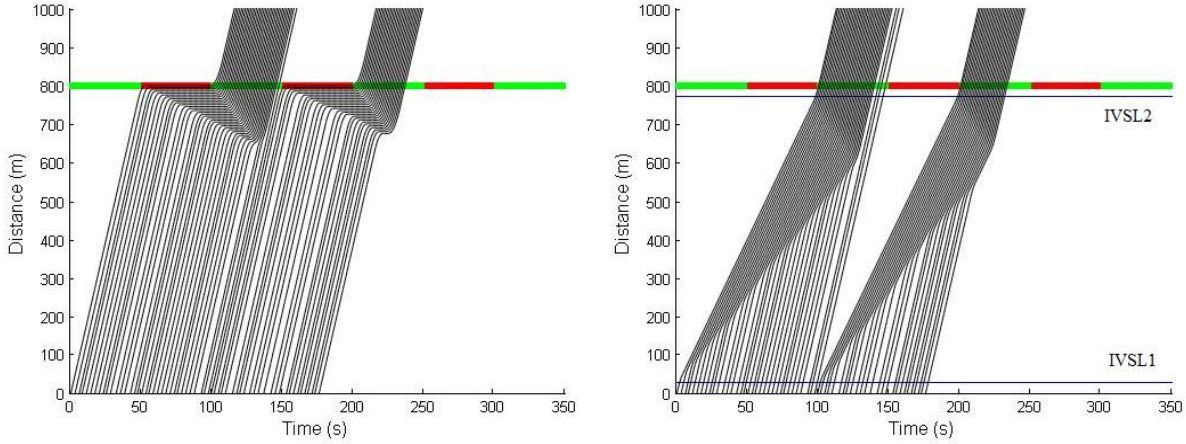

Benchmark IVSL-SO

b) Intermediate traffic scenario.

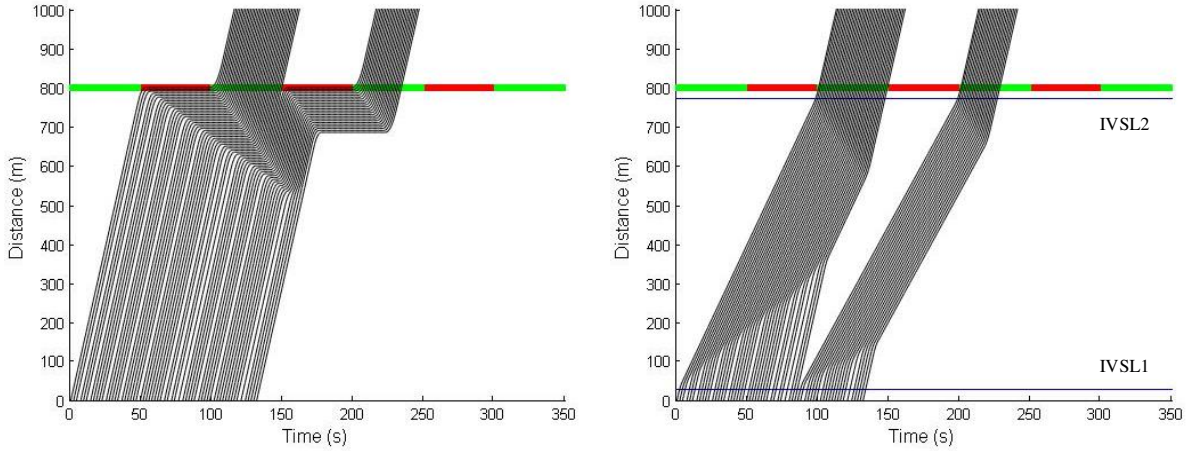

Benchmark IVSL-SO

c) Dense traffic scenario.

Figure 10 Time-space trajectories with/without control under specific scenarios.

5. Conclusion

In this paper, we first investigate the impacts of different car-following models with the deterministic IVSL strategy in a CV environment at a signalized intersection. Then, we propose a stochastic IVSL model as a two-stage optimization problem considering the stochastic vehicle arriving patterns. To solve this problem, we apply the Monte Carlo framework with the DIRECT algorithm. A set of numerical experiments is conducted to test the model performance. Regarding different car-following models (i.e., the Gipps' model, the revised Newell's model, and the IDM model), results show that the Gipps' model yields better results than the other models. This is probably because the safety features are considered in Gipp's model, which is more realistic. Further, the stochastic IVSL model is verified that can improve 8.95% travel time, 19.11% fuel consumption, and 11.37% system cost compared to the benchmark without speed control.

Although the proposed model yields valuable benefits in terms of travel time, fuel consumption, and system cost, several research directions can be extended from this work. First, this paper only considers the longitudinal motions in a single-lane road. The lateral motions (e.g., lane changing behaviors) should be considered in the future. Second, this paper only considers a small-scale problem with an isolated signalized intersection. It is valuable to investigate the speed control strategy on a larger scale (e.g., corridors and networks).

Declaration

The authors declare that they have no conflict of interest, and this manuscript is original and has not been published or submitted elsewhere for publication.

Author Contributions: The authors confirm their contribution to the paper as follows. Study conception and design—Handong Yao; data collection— Qianwen Li and Handong Yao; analysis and interpretation of results—Qianwen Li; draft manuscript preparation—Qianwen Li and Handong Yao. All authors reviewed the results and approved the final version of the manuscript.

References

Ahn, K. (1998). "Microscopic fuel consumption and emission modeling."

Gipps, P. G. (1981). "A behavioural car-following model for computer simulation." Transportation Research Part B: Methodological **15**(2): 105-111.

He, X., H. X. Liu and X. Liu (2015). "Optimal vehicle speed trajectory on a signalized arterial with consideration of queue." Transportation Research Part C: Emerging Technologies **61**: 106-120.

Jamson, A. H., D. L. Hibberd and N. Merat (2015). "Interface design considerations for an in-vehicle eco-driving assistance system." Transportation Research Part C: Emerging Technologies **58**: 642-656.

Jiang, H., J. Hu, S. An, M. Wang and B. B. Park (2017). "Eco approaching at an isolated signalized intersection under partially connected and automated vehicles environment." Transportation Research Part C: Emerging Technologies **79**: 290-307.

Jones, D. R., C. D. Perttunen and B. E. Stuckman (1993). "Lipschitzian optimization without the Lipschitz constant." Journal of Optimization Theory and Applications **79**(1): 157-181.

Kamalanathsharma, R. K. and H. Rakha (2012). Agent-based modeling of eco-cooperative adaptive cruise control systems in the vicinity of intersections. Intelligent Transportation Systems (ITSC), 2012 15th International IEEE Conference on, IEEE.

Katsaros, K., R. Kernchen, M. Dianati and D. Rieck (2011). Performance study of a Green Light Optimized Speed Advisory (GLOSA) application using an integrated cooperative ITS simulation

platform. Wireless Communications and Mobile Computing Conference (IWCMC), 2011 7th International, IEEE.
Koonce, P., L. Rodegerdts, K. Lee, S. Quayle, S. Beaird, C. Braud, J. Bonneson, P. Tarnoff and T. Urbanik (2008). Traffic signal timing manual.
Li, L., S. You, C. Yang, B. Yan, J. Song and Z. Chen (2016). "Driving-behavior-aware stochastic model predictive control for plug-in hybrid electric buses." Applied Energy **162**: 868-879.
Li, W., G. Wu, M. J. Barth and Y. Zhang (2016). Safety, mobility and environmental sustainability of Eco-Approach and Departure application at signalized intersections: A simulation study. Intelligent Vehicles Symposium (IV), 2016 IEEE, IEEE.
Liu, B., D. Ghosal, C. N. Chuah and H. M. Zhang (2012). "Reducing Greenhouse Effects via Fuel Consumption-Aware Variable Speed Limit (FC-VSL)." IEEE Transactions on Vehicular Technology **61**(1): 111-122.
Ma, J., X. Li, F. Zhou, J. Hu and B. B. Park (2017). "Parsimonious shooting heuristic for trajectory design of connected automated traffic part II: Computational issues and optimization." Transportation Research Part B: Methodological **95**: 421-441.
Mahler, G. and A. Vahidi (2012). Reducing idling at red lights based on probabilistic prediction of traffic signal timings. American Control Conference (ACC), 2012, IEEE.
May, A. D. (1990). Traffic flow fundamentals.
Metropolis, N. and S. Ulam (1949). "The monte carlo method." Journal of the American statistical association **44**(247): 335-341.
Newell, G. F. (2002). "A simplified car-following theory: a lower order model." Transportation Research Part B Methodological **36**(3): 195-205.
Nguyen, V., O. T. T. Kim, T. N. Dang, S. I. Moon and C. S. Hong (2016). An efficient and reliable Green Light Optimal Speed Advisory system for autonomous cars. Network Operations and Management Symposium (APNOMS), 2016 18th Asia-Pacific, IEEE.
Pampel, S. M., S. L. Jamson, D. L. Hibberd and Y. Barnard (2015). "How I reduce fuel consumption: An experimental study on mental models of eco-driving." Transportation Research Part C: Emerging Technologies **58**: 669-680.
Rakha, H., H. Chen, M. Almannaa, R. K. Kamalanathsharma, I. El-Shawarby and A. Loulizi (2016). "Field Testing of Eco-Speed Control Using V2I Communication."
Sun, J. and H. X. Liu (2015). "Stochastic eco-routing in a signalized traffic network." Transportation Research Procedia **7**: 110-128.
Tong, Y., L. Zhao, L. Li and Y. Zhang (2015). "Stochastic programming model for oversaturated intersection signal timing." Transportation Research Part C: Emerging Technologies **58**: 474-486.
Treiber, M., A. Hennecke and D. Helbing (2000). "Congested traffic states in empirical observations and microscopic simulations." Physical review E **62**(2): 1805.
Treiber, M. and A. Kesting (2013). "Traffic flow dynamics." Traffic Flow Dynamics: Data, Models and Simulation, Springer-Verlag Berlin Heidelberg.
Ubiergo, G. A. and W.-L. Jin (2016). "Mobility and environment improvement of signalized networks through Vehicle-to-Infrastructure (V2I) communications." Transportation Research Part C: Emerging Technologies **68**: 70-82.
Wan, N., A. Vahidi and A. Luckow (2016). "Optimal speed advisory for connected vehicles in arterial roads and the impact on mixed traffic." Transportation Research Part C: Emerging Technologies.
Weibull, W. (1951). "Wide applicability." Journal of applied mechanics **103**: 33.
Xiang, X., K. Zhou, W.-B. Zhang, W. Qin and Q. Mao (2015). "A Closed-Loop Speed Advisory Model With Driver's Behavior Adaptability for Eco-Driving." IEEE Transactions on Intelligent

Transportation Systems **16**(6): 3313-3324.
Yang, H., H. Rakha and M. V. Ala (2016). "Eco-Cooperative Adaptive Cruise Control at Signalized Intersections Considering Queue Effects." IEEE Transactions on Intelligent Transportation Systems.
Yao, H., Cui, J., Li, X., Wang, Y., and An, S. (2018). "A trajectory smoothing method at signalized intersection based on individualized variable speed limits with location optimization." Transportation Research Part D: Transport and Environment, 62, 456-473.
Zegeye, S., B. De Schutter, J. Hellendoorn, E. Breunesse and A. Hegyi (2013). "Integrated macroscopic traffic flow, emission, and fuel consumption model for control purposes." Transportation Research Part C: Emerging Technologies **31**: 158-171.
Zhou, F., X. Li and J. Ma (2017). "Parsimonious shooting heuristic for trajectory design of connected automated traffic part I: Theoretical analysis with generalized time geography." Transportation Research Part B: Methodological **95**: 394-420.